Nanofibrillar Structure and Molecular Mobility in Spider Dragline Silk

D. Sapede,[†,‡] T. Seydel,[†] V. T. Forsyth,[†,⊥] M. M. Koza,[†] R. Schweins,[†] F. Vollrath,[§] and C. Riekel*[,‡]

Institut Max von Laue-Paul Langevin, B.P. 156, F-38042 Grenoble, France; European Synchrotron Radiation Facility, B.P. 220, F-38043 Grenoble, France; Department of Zoology, University of Oxford, South Parks Road, Oxford OX1 3PS, U.K.; and Institute for Science and Technology in Medicine, Keele University Medical School, ST4 7QB, U.K.

Received April 14, 2005; Revised Manuscript Received July 22, 2005

ABSTRACT: *Nephila edulis* dragline silk has been investigated by elastic and quasielastic neutron scattering techniques. The data support a three-phase model of nanofibrils, composed of crystalline and short-range order domains, which are embedded in an amorphous matrix of random protein chains. A meridional superlattice peak in D_2O-exchanged silk is tentatively assigned to a smectic β-sheet structure in the short-range order domains. Water is absorbed preferentially by the amorphous matrix. The onset of molecular mobility in hydrated silk at about 200 K is attributed to water molecules, which move on the picosecond time scale. Coexisting slower motions on the nanosecond time scale are possibly due to polymer chain dynamics. Native silk at rest appears to behave similar to a glass below 300 K.

Introduction

Spider dragline silk is a semicrystalline fiber, which is made of proteins containing repeating sequence motifs.[1−4] *Nephila clavipes* silk is assumed to be made up from the proteins spidroin 1[1] and spidroin 2[4] which contain repeat motifs of polyalanine blocks separated by glycine-rich sequences. The crystalline fraction of the fiber is composed mainly of the polyalanine blocks and the amorphous fraction of the glycine-rich sequences. Dragline silk fibers combine remarkable elasticity and strength, which allows dissipating the kinetic energy of the insects to be captured.[2,5] These outstanding mechanical properties are obtained for a material spun from aqueous solution close to ambient temperature and pressure.[6] A detailed understanding of the hierarchically organized material[7] requires the understanding of the structural and viscoelastic properties on length scales down to the molecular level. Microscopic models have been obtained principally from electron scattering,[8−11] X-ray/synchrotron radiation (SR) scattering,[12−23] atomic force microscopy (AFM),[7,24,25] and spectroscopic techniques such as IR,[26] Raman,[27−29] and NMR.[30−38] Thus, wide-angle X-ray scattering (WAXS) favors the presence of small crystalline domains (<10 nm) in a matrix of random protein chains.[15,18,19] The observation of short-range order suggests the presence of a further constrained chain fraction.[15,18] Constrained chains at the interface of the crystalline domains to the random matrix are also assumed in molecular modeling studies.[39] X-ray small-angle scattering (SAXS) suggest the existence of nanofibrillar objects composed of crystalline and short-range order domains with an average fibrillar period of 7−8 nm, which remain present during hydration.[16,21,22]

Compared to X-rays, neutrons show a much stronger interaction with hydrogen atoms[40] which implies that neutron scattering techniques are particularly sensitive to hydration-related changes in microscopic structure and dynamics. We refer in particular to experiments on polyamides, such as nylon-6, which resemble in several aspects dragline silks as they form interchain hydrogen bonds due to secondary amide groups −NHCO− in the chains and show hydration processes and a lamellar SAXS peak.[41−43] The model character of such homopolymer studies is, however, limited due to the more complex molecular structure and morphology of dragline silks.

To contribute to a refinement and extension of existing structural models, both small-angle (SANS) and wide-angle neutron scattering (WANS) experiments were performed on highly aligned spider dragline silk fiber bundles in order to probe the structural organization on several hierarchical levels. The interpretation of these data in terms of microscopic models is enhanced by numerical methods. The control of the level of humidity and the H/D ratio of the solvent allows testing the accessibility of the different structural elements of the fibers to water. It can be assumed that an understanding of both structural and dynamical properties of the silk is essential to elucidate the remarkable mechanical and viscoelastic properties. In particular, the knowledge on the state of water and of force fields in the fibers may contribute to a deeper understanding. Complementary neutron spectroscopic experiments, probing an equivalent hierarchy of dynamical processes down to molecular length scales, were therefore performed.

Experimental Section

Materials. Silk fibers were collected by the forced silking technique[44] from *Nephila edulis* spiders, which were reared in-house at Oxford.[45] Spiders were anesthetized only lightly and well prior to silking in order to avoid an influence on the microstructural properties of the silk.[21,45] All experiments reported below were carried out within ∼1 year, and the samples were stored under cool and dry conditions. Small pieces of fibers from the samples were checked by SR microdiffraction,[18] and no indication of degradation was observed.

Neutron Scattering. Neutron scattering experiments were performed at the high-flux reactor of the ILL. Wide-angle neutron scattering (WANS) experiments were performed at the D19 beamline at a wavelength of $\lambda = 0.24$ nm.[46] A ^{3}He gas-filled detector with 64 × 64 pixels with 200 mm^2 active area was used. For a sample-to-detector distance of 567.67 mm, an angle of 20° was covered. A full fiber diffraction pattern

[†] Institut Max von Laue-Paul Langevin.
[‡] European Synchrotron Radiation Facility.
[§] University of Oxford.
[⊥] Keele University.
* Corresponding author.

10.1021/ma0507995 CCC: $30.25
Published on Web 09/10/2005

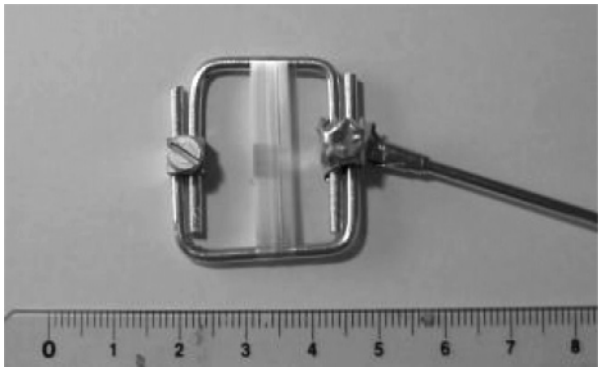

Figure 1. Photograph of spider dragline silk (mass about 20 mg) wound on an aluminum frame sample holder.

up to 2Θ angle of 60° was covered in 28 detector positions corresponding to 18.5 h recording time. Small-angle neutron scattering (SANS) experiments were performed with the D11 and D22 pinhole cameras.[46] D11 was operated at a wavelength of $\lambda = 0.6$ nm and a sample-to-detector distance of 1500 mm. A gas-filled detector with 64 × 64 pixels and 10 × 10 mm^2 pixel size was used. The data were corrected to obtain absolute intensities using a standard approach.[47] The D11 data were used to study the influence of the hydration state and the H/D exchange ratio on the patterns. D22 was operated at a wavelength of $\lambda = 0.6$ nm with detector-to-sample distances of 17 000, 6000, and 1400 mm, which allowed increasing the separation of the meridional peak from the beamstop. A gas-filled detector with 128 × 128 pixels and 7.5 × 7.5 mm^2 pixel size was used. The data were corrected for cell background and detector noise and were normalized to 600 s counting time. These data were used to obtain the highest possible resolution. SANS and WANS patterns were displayed using the FIT2D software.[48] Reflection intensities were fitted using one-dimensional (1D) or two-dimensional (2D) Gaussian functions and zero- or first-order polynomial backgrounds. Intensities were integrated in radial direction within the segment of an annulus in order to determine 1D intensity profiles. 2D fits were performed for the azimuthally regrouped patterns.

Quasielastic scattering experiments (QNS) were carried out using the IN16 backscattering spectrometer as well as the IN6 time-of-flight spectrometer.[46] IN6 allowed in addition for measuring the vibrational excitations (i.e., inelastic scattering), which, however, are not discussed in this article. IN16 was used in the configuration with Si111 analyzer crystals corresponding to a wavelength of 0.627 nm. With IN16 an energy transfer range of about $\Delta E = \pm 14$ μeV for QNS scans, with an elastic energy resolution of about 0.9 μeV fwhm and a Q range of about 0.2−19 nm^{-1}, could be covered. IN6 was used at an incident wavelength of 0.51 nm to extend the energy range to about 100 meV with an elastic energy resolution of about 70 μeV fwhm. The QNS data were analyzed by using the software packages LAMP and IDA provided by ILL and subsequently MATLAB scripts.

Sample Environment. The silk was wound on aluminum frames (Figure 1). For cryostated and controlled-humidity environments, the frames were put in specially designed sample aluminum containers. Experiments were performed in general with the fiber axis perpendicular to the scattering plane. A typical experiment was performed with about 150 mg of silk, and some SANS data were obtained with about 20 mg of silk. WANS and SANS experiments were performed at room temperature with the sample exposed to a constant stream of humidified gas of 75% relative humidity. This environment was also used to perform H/D exchange experiments by placing for example a D_2O-humidified sample at $t = 0$ in a constant stream of H_2O-humidified airflow. QNS experiments were performed with the sample inside a cryostat allowing for a temperature range of 2−320 K. In addition, the sample could be humidified and dried in situ via heatable capillaries inside an evacuated cane that connected the sample container with valves outside the cryostat. For the QNS experiments it was possible to adjust a certain humidity level reproducibly on the basis of the QNS intensity of the measured spectra by pumping in situ on a humid sample. We verified by WAXS experiments at the ESRF ID13 beamline that hydrated fibers did not form crystalline ice down to 100 K.[18]

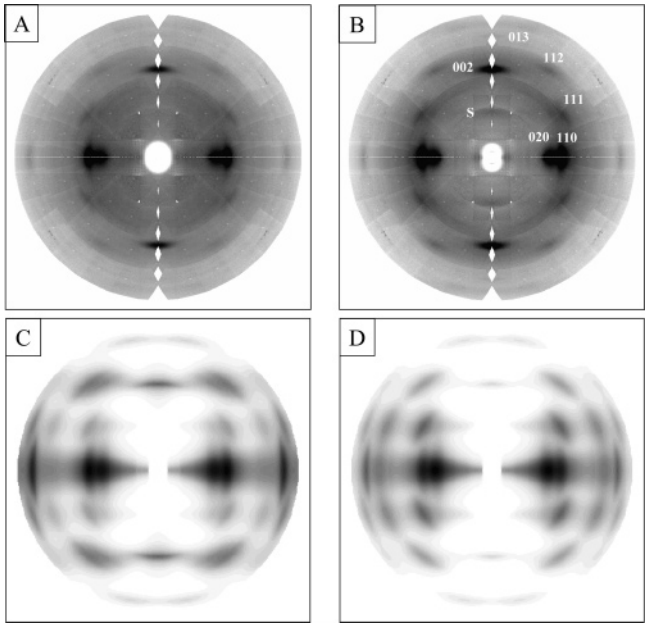

Figure 2. (A) Neutron fiber diffraction pattern of H_2O-humidified dragline silk. (B) Neutron fiber diffraction pattern of D_2O-humidified silk. The gaps along the meridian are blind regions in reciprocal space corresponding to the tilt series used in data collection. Indices of strongest reflections according to Arnott et al.,[50] S is a diffuse superlattice peak appearing at the position of the (forbidden) 001 reflection. (C) Simulated neutron fiber diffraction pattern of H-polyalanine for $\lambda = 0.24$ nm neutrons. (D) Simulated pattern of D-polyalanine (same scale for both patterns).

Results and Discussion

Crystalline Fraction and Its H/D Exchange. The neutron fiber diffraction patterns of silk humidified with H_2O and D_2O (Figure 2A,B) resemble in general the X-ray patterns.[49] The reflection intensities are similar and correspond to the β-poly(L-alanine) structure (abbr: polyalanine).[50,51] We note, however, a diffuse superlattice reflection (S) appearing in the D_2O-exchanged pattern at the position of the 001 reflection (lattice spacing of $d \approx 0.7$ nm), which is not allowed for the orthorhombic $C222_1$ or $P2_12_12_1$ space groups derived from X-ray data.[50,51] In addition, a powder ring due to water and random chains is present.[12]

The influence of the H/D ratio on the patterns was calculated using the Cerius^2 software (Accelrys) for the polyalanine structure by Arnott et al.[50] (Figure 2C,D). It was assumed that an H/D exchange could only occur for the N−H group, and the CH_3 side group was kept rigid for simplicity. The simulations demonstrate the strong influence of the H/D exchange on the equatorial reflections 110/020. A ratio of integrated intensities $I_{110}/I_{020} = 0.95$ was calculated for H-polyalanine (N−H group) and $I_{110}/I_{020} = 0.39$ for D-polyalanine (N−D group). Experimentally determined values of $I_{110}/I_{020} = 1.1$ for H-polyalanine and $I_{110}/I_{020} = 1.2$ for D-polyalanine are practically identical, given the uncertainty in background subtraction due to the presence of amorphous material.[18] We conclude that the crystalline H-polyalanine fraction shows only a negligible H/D exchange.

Evidence for Smectic Order. The superlattice (S) and 002 reflections shown in Figure 2B were fitted using

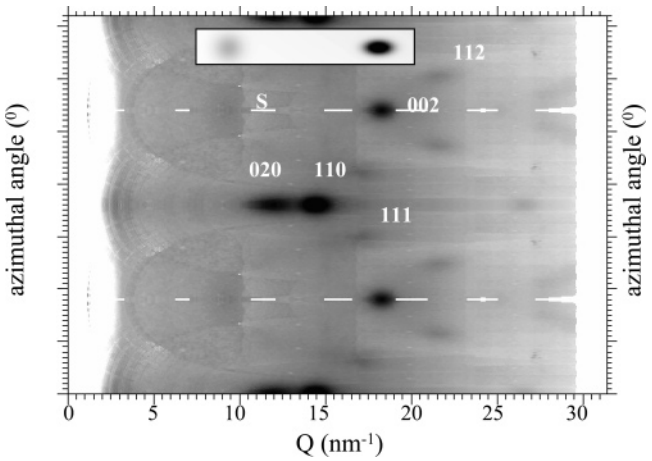

Figure 3. Cake-regrouped neutron fiber diffraction pattern of D_2O-humidified silk (Figure 2B). The inset shows the 2D-Gaussian profiles of the simulated 002 reflection and superlattice peak ($Q = 2\pi/d$).

2D Gaussian profiles and a first-order polynomial background (Figure 3). The ratio of integrated intensities was derived from the fit as $I_S/I_{002} = 0.36$. We note that the azimuthal width of 36.2° fwhm of the superlattice reflection derived from the fit is significantly larger than for the 002 reflection (16.8° fwhm). The azimuthal width of the meridional 00l (or hk0) reflections can be related to an axial orientation distribution of crystalline domains.[15,18] This does, however, not provide an explanation for the enlarged width of the superlattice peak. We also consider the assumption of crystal defects[52] resulting in a breakdown of the $l = 2n$ extinction as less probable as it has never been observed by SR diffraction experiments on a range of dragline silks.[18,49] The presence of the superlattice peak is therefore also difficult to reconcile with a different space group or a superstructure due to a repetitive sequence of other residues, such as serine residues in silk fibroin.[51,53,54] This also holds for the assumption of a more or less random distribution of β-sheet nuclei[34] in the amorphous matrix, which is incompatible with the meridional position of the superlattice reflection. We note, however, that the azimuthal width of the superlattice reflection corresponds to the broadening of the oriented equatorial halo due to short-range order as seen by WAXS, which can be separated from the 210 reflection by profile fits.[15,18] The azimuthal widths of both WAXS peaks show considerable variability during artificial drawing of dragline silk, which can be related to variations in drawing stress and possibly mechanical action within the spinnerets.[19,20] Dragline protein chain-folding models suggest an aggregation of alanine sequences through a backfolding of β-strands via serine−glycine or glycine−asparagine "hairpin loops".[4,12,34,55] We tentatively assume that the glycine-rich chains, which do not participate in the formation of a polyalanine block, are constrained into a smectic β-sheet structure, which is laterally disordered due to a mismatch of side groups. A larger orientation distribution of chain axes in the smectic phase would explain the increased azimuthal width of the superlattice reflection as compared to the crystalline domains 002 reflection. Note that for certain amyloid cross-β systems the side groups interlock, and 3D structures are formed.[56] The 0.7 nm superlattice reflection corresponds therefore for a smectic model to the repeating chain unit in the short-range order domains. The presence of nanofibrillar objects composed of crystalline domains separated by short-range order domains can be deduced from SANS patterns and will be discussed in more detail below. One can show that the alanine molecules of the principal silk protein molecules "fill up" roughly a single crystalline domain.[12] This suggests that the formation of nanofibrils could occur through an aggregation across a "fold surface", which is assumed to form at both sides of each polyalanine domain[12] and resembles solution grown polymer single crystals.[57]

Contrast Variation of Amorphous Fractions. Spider dragline silk is readily absorbing water by its amorphous network which results in a breaking of the hydrogen-bonded network[39] and an increase in kinetic freedom of the chains.[58] The meridional SAXS peak[16,22,23] suggests in addition the presence of semicrystalline nanofibrillar objects, which act as reinforcing network elements. The presence of water in the fiber can be directly observed by SAXS/WAXS techniques during major ampullate silk extrusion.[22] The slight variation of the long period peak of the nanofibrils during hydration[16,21] suggests also an incorporation of water molecules into the short-range order fraction although the constrained environment will probably limit this to the immediate neighborhood of the chains.

A unique feature of SANS experiments is that the meridional peak observed in D_2O solvent is practically extinguished in H_2O (Figure 4A). The kinetics of this H/D exchange can be fitted by a first-order exponential decay with a decay constant of $\tau = 15.8$ min (Figure 4B). No evidence for a discrete equatorial peak of 4.5 nm, which has been observed by SAXS for dry *Nephila clavipes* silk,[59] was obtained in the hydrogenated or deuterated materials. The variations of the integrated intensities of the meridional peak and the equatorial streak as a function of the D_2O content of the solvent are shown in Figure 4C.

For modeling of the meridional SANS peak profile a single Gaussian function and a first-order polynomial background were used. Peak positions corresponding to d values of 7.2 nm for the dried sample and 7.6 nm for the humid sample agree well with SAXS experiments.[16,21,22] A second-order peak observed in SAXS experiments on more or less dry silk[16,21] is, however, not present. Both profiles show the same radial width, suggesting no significant changes in domain size due to hydration, which agrees also with the WANS experiments.

The variation of the integrated intensities of the meridional peak and the equatorial streak as a function of the D_2O content of the solvent are shown in Figure 4C. The discussion will be limited to a qualitative analysis of the intensity variations. More quantitative simulations (such as performed for the analogue case of lamellar starch granules[60]) are beyond the scope of the present article. Thus, the meridional "long period" peak is attributed to a sequence of crystalline (alanine-rich) and short-range order (glycine-rich) domains in the nanofibrils.[12,16,22] For a long period of about 7−8 nm (see below) and a crystalline domain size of about 4 nm along the nanofibrils axis,[22] this results in a size of the short-range order domains of 3−4 nm. The intensity of the meridional peak is given in the SANS case by

$$I(Q) = k\Delta_{sld}{}^2|P_c(Q)|^2Z(Q) \qquad (1)$$

where k is a normalization constant, $\Delta_{sld} = \overline{C_{sld}} - \overline{A_{sld}}$ is the mean scattering length density difference between

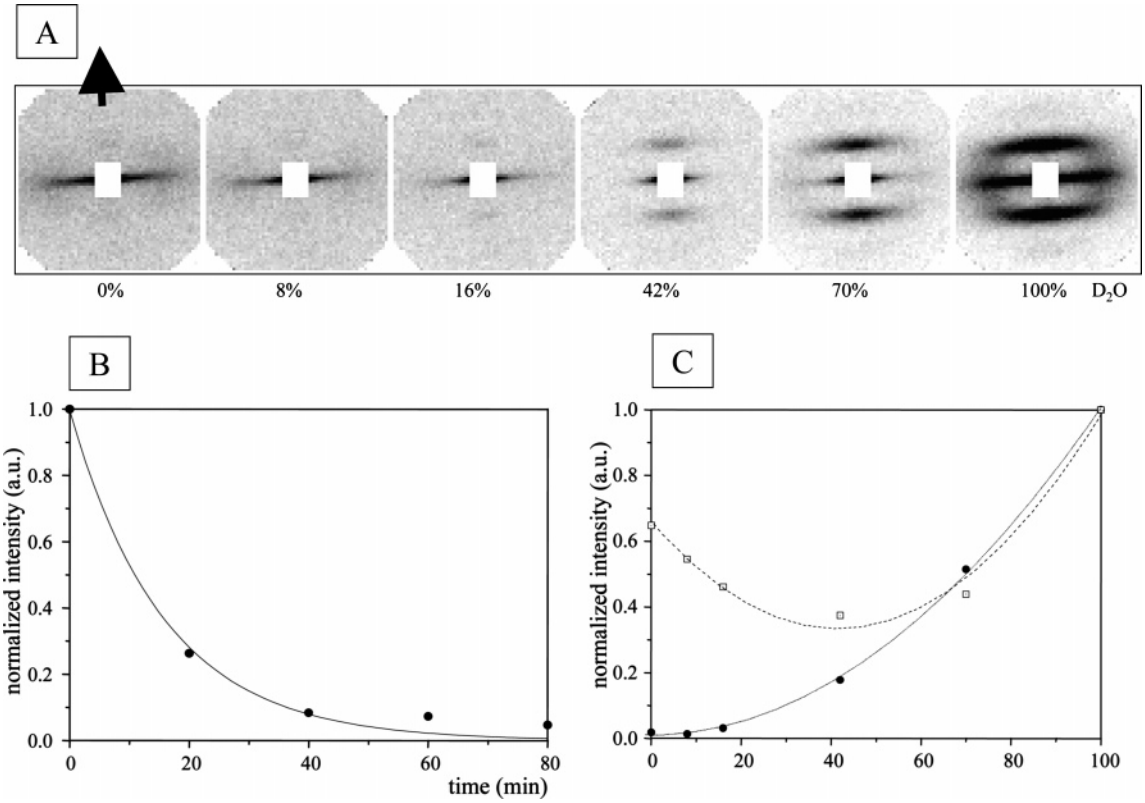

Figure 4. (A) Influence of H/D ratio on SANS patterns (the equator is oriented horizontally). An arrow shows the direction of the macroscopic fiber axis. (B) Kinetics of H/D exchange from variation of integrated meridional peak intensity. (C) Integrated equatorial streak (open rectangles) and integrated meridional peak (full circles) as a function of the D_2O content of the solvent. Polynomial functions were fitted for guiding the eye.

crystalline and short-range order domains, P_c is the form factor of a crystalline domains, and $Z(Q)$ is the Laue interference function.[61] The variation of meridional intensity with H/D ratio of the solvent depends principally on the variation of the scattering length term. The H/D exchange on the chains will affect practically only the polyglycine N−H groups in the short-range order domains, which are accessible to solvent molecules. An exchange on the chains is also suggested by the meridional superlattice peak, which is only observed for the D_2O-exchanged material (Figure 2B). The total scattering lengths of H-polyalanine (1.645×10^{-12} cm/molecule) and H-polyglycine (1.728×10^{-12} cm/molecule) are similar, which results in a virtual extinction of the meridional peak for H_2O as solvent.[62] The exchange to D-polyglycine (2.769×10^{-12} cm) introduces a Δ_{sld} increase, which shows up in an increase of the meridional peak intensity. Constrained water in the short-range order domains will further increase Δ_{sld}. Thus, a "decoration" of the N−H groups by water molecules would change the total scattering length of H-polyglycine to 1.56×10^{-12} cm and of D-polyglycine to 4.684×10^{-12} cm. A fraction of water entering the short-range order domains is suggested by the dependence of the lamellar spacing on the hydration state.[16,21]

In contrast, the intensity of the equatorial streak is proportional to the product of the nanofibrils form factor $P_n(Q)$ and the contrast $\Delta\rho^*$ due to the scattering length density difference between nanofibrils and surrounding random matrix:

$$I(Q) = k' P_n(Q) \Delta\rho^* \qquad (2)$$

This has been discussed in more detail for SAXS data for cellulose nanofibrils in flax.[63] Water molecules entering the more or less dry random silk matrix will reduce its density and hence increase the $\Delta\rho^*$ term, which is readily observed for in-situ SAXS experiments.[21,22] For SANS the H/D exchange will affect $\Delta\rho^*$ through the variation of the scattering length density of the nanofibrils and of the solvent in the matrix. Figure 4C shows that the equatorial streak reaches a minimum at about 40% D_2O, which corresponds roughly to the match point for proteins.[62] The match point of the exchangeable glycine is at about 50% D_2O while the match point for H-alanine is at about 30% D_2O. The observed minimum corresponds therefore to a compromise between the exchangeable and the nonexchangeable fractions.

We note that the H/D exchange inferred from SANS data is generally supported by NMR experiments, which do not, however, distinguish between short-range order and amorphous fractions[31,35,38] as is also the case for Raman spectroscopy.[28]

Nanofibrillar Dimension. A detailed analysis of the equatorial streak of *Nephila* silk recorded by SAXS in terms of orientation and dimensions of nanofibrillar objects has already been reported.[16] The SANS data obtained for dry silk kept at atmospheric humidity at D22 support this analysis although the data extend to smaller Q values. The broadening was determined at selected Q values parallel to the meridional axis by fitting Gaussian functions to the peak profiles. The data obtained at the 17 m detector distance show that a single Gaussian function allows fitting the equatorial streak up to about $Q \approx 0.26$ nm^{-1} while the width of the streak is decreasing to a constant value of ≈8° fwhm (Figure 5A). At larger Q values a second broader (≈26°

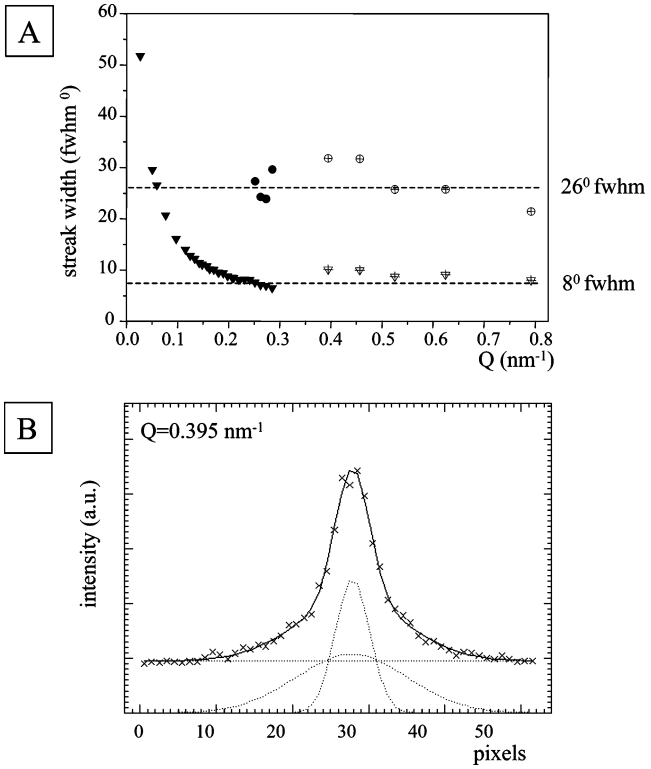

Figure 5. (A) Angular width of equatorial streak as a function of scattering vector Q. A single Gaussian function could be fitted to the streak up to $Q \approx 0.26$ nm^{-1}. For higher Q values two Gaussian functions had to be used. Filled symbols correspond to data obtained at the 17.0 m detector position and open symbols to the 6.0 m detector position. (B) The presence of a narrow and a broad peak is shown for the streak at $Q = 0.395$ nm^{-1}. Crosses correspond to experimental data and solid lines to the fits.

fwhm) Gaussian function is required to model the streak (Figure 5B). The data at the 6 m detector position confirm these two peaks and allow extending the fits to larger Q values (Figure 5A). These results support the previous SAXS analysis,[16] which assumes that the streak width is dominated at the smallest Q values by the dimension of the nanofibrillar objects and at higher Q values by their orientation. Thus, the two peak widths observed suggest the presence of two types of nanofibrillar domains differing in chain orientation distribution. The low-Q tail was attributed to central scattering due to larger scale features such as crazes.[16] This is a reasonable assumption as *Nephila* silk contains elongated cavities oriented parallel to the silk fiber axis.[64] The rise of the central scattering starts at about $Q \leq 0.25$ nm^{-1} (Figure 5A). Following the SAXS analysis,[16] a streak width of 8° corresponds at $Q = 0.25$ nm^{-1} to $\Delta Q = 0.033$ nm^{-1} fwhm. The lower limit in nanofibrillar dimensions in axial direction (L) can be derived from the Scherrer formula[65] via $L = 1.8\pi/\Delta Q$ as about 170 nm. For a repeating unit of about 7.5 nm this corresponds to about 22 units along the nanofibrillar axis. Interestingly, based on birefringence experiments, a similar number of units has been discussed for rodlike aggregates in liquid crystalline silk secretions.[66] We speculate therefore that these nanofibrils are the basic building blocks for the fiber formation in dragline silk and are already predefined during the first aggregation steps of globular proteins in the liquid crystalline phase. A more detailed analysis in terms of an orientation function[15,18] will not be attempted in view of the strong dependence of the orientation distribution on the external strain, which depends on the hydration state of the fiber bundle.[15,19,20]

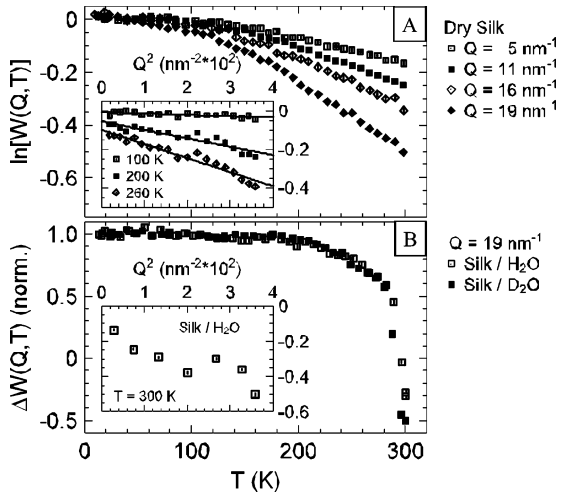

Figure 6. (A) Intensity plotted as ln[$W(Q,T)$] measured with a "fixed energy window" scan centered at zero energy transfer as a function temperature for different values of the scattering vector Q. In the insets, the corresponding Q dependence is plotted at fixed temperatures 100, 200, and 260 K. (B) Difference signal of humid minus native dry silk shown at a single Q for deuterated and protonated water. The inset shows the Q dependence measured at 300 K in the H_2O humidified silk.

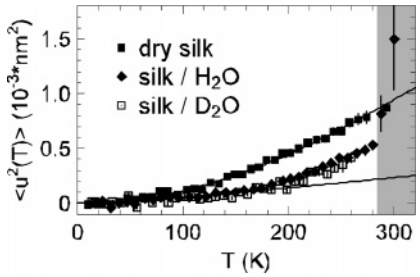

Figure 7. Mean-square displacement of the scatterers $\langle u^2(T)\rangle$ obtained by fitting the assumption $I = I_0 \exp(-\langle u^2\rangle Q^2) + c$ to the data, i.e., the slopes in the insets of Figure 6A. Full lines indicate the behavior expected for harmonic solids and matched to the data of dry silk and humidified with protonated water. The gray shaded area stresses the temperature range in which the $\langle u^2(T)\rangle$ of humidified silk exceeds $\langle u^2(T)\rangle$ of the dry sample.

Molecular Mobility. An overview of dynamical phenomena in a sample can be obtained by "fixed energy window" (FEW) scans, where the intensity scattered within the energy resolution window of the spectrometer is recorded. FEW scans centered at zero energy transfer (also called "elastic scans") were obtained on IN16 from air-dry and H_2O/D_2O humidified silk samples (Figure 6A,B). The silk fiber axis was perpendicular to the scattering plane of the spectrometer. Data on the native silk sample are reported in Figure 6A. For silk humidified with H_2O and D_2O, difference spectra (native silk subtracted) are displayed in Figure 6B. Assuming a simple $W(Q,T) = \exp(-\langle u^2(T)\rangle Q^2)$ dependence of the elastic intensity, the mean-square displacement ($\langle u^2(T)\rangle$) of the scatterers can be calculated from the Q dependence of $W(Q,T)$, as is indicated in the inset of Figure 6A,B. The such obtained $\langle u^2(T)\rangle$ data are reported in Figure 7 for native and humidified samples.

In the case of the native silk the linear Q^2 dependence of $W(Q,T)$ and the overall temperature dependence of $\langle u^2(T)\rangle$ are reminiscent of the properties of a harmonic

system. By contrast, in the humidified samples the behavior is nonharmonic above ~200 K. This feature may tentatively be attributed to a gradual melting of amorphous water. Since no sharp transition can be identified, this melting behavior is unlike in systems with well-defined pore sizes. It rather looks like a continuous melting process resulting from water confined in a hierarchy of pore sizes within the random network of the amorphous silk fraction. The response of the frozen-in state of both H_2O and D_2O humidified silk at $T < 200$ K can be well compared with the behavior of amorphous ice,[67−69] marking the system as harmonic and more rigid than the native silk, which is evidenced by the smaller $\langle u^2(T)\rangle$ values.

The enhanced $\langle u^2(T)\rangle$ of the humidified samples at room temperature may not be exclusively attributed to relaxation of water molecules within the amorphous silk matrix. The confined water equally opens up decay channels for the polymer chains. This point can be clearly elaborated by subtracting the response of the native silk from the humidified samples $\Delta W(Q,T) = W_{\text{humid}}(Q,T) - W_{\text{native}}(Q,T)$. In a simplified picture of a separate water and polymer dynamics one would expect $\Delta W(Q,T)$ to be dominated by the water response and to remain a positive property. However, as can be judged from Figure 6B, the $\Delta W(Q,T)$ becomes appreciably negative at room temperatures. This can be only the case when the humid samples comprise a remarkably higher degree of decay channels than liquid water at equal thermodynamic conditions. In other words, the mobility of polymer chains is enhanced by the presence of water.

It is obvious from the FEW experiments that the classification of relaxation processes from experimental data only is bound to fail in a system displaying such a structural and dynamic complexity like the humidified silk. For example, when taking confined water into consideration, a discrimination between different diffusion channels requires well-defined geometry and dimensions of the confining media. None of these requirements are fulfilled in the apparently hierarchically structured silk fibers.

We may draw at least conclusions upon the time scales of the relaxation processes from the quasielastic signal recorded on the spectrometers IN6 and IN16. The humidified samples display already at 250 K a quasielastic signal that spans time scales of some nanoseconds (IN16) to picoseconds (IN6), i.e., at temperatures at which water is still partially frozen. At room temperature the intensity of the quasielastic signal is appreciably increased in accordance with the FEW measurements pointing at a higher number of scatterers taking part in the relaxation of the samples. We cannot, however, unequivocally confirm a change in dynamics that could be for example expected due to a higher mobility of the polymers setting off at elevated temperatures. The separation of the dynamic responses of the polymer matrix and the confined water constitutes indeed a grave experimental challenge, which will be tackled in future studies.

Conclusions and Outlook

With the neutron scattering experiments on spider dragline silk reported in this article we have established the feasibility of neutron spectroscopic and small-angle scattering techniques on a biopolymer that is only available in limited quantities and that poses a challenge to the pursuit of understanding its mechanical properties. Our study may provide a benchmark for the study of other fibrous biopolymers using neutrons.

In a simplified picture, a spider dragline silk fiber even at ambient temperature and ambient humidity closely resembles to a network with reinforcing nanofibrillar elements. Such a model has already been proposed previously[15,39] and is thus in agreement with our neutron scattering experiments. Absorption of water does not modify the morphology significantly although additional diffuse scattering in the hydrated sample suggests a new type of short-range order. The presence of water appears, however, to noticeably modify the dynamical properties of the polymer matrix, although further information has yet to be obtained.

The present report provides the basis for a more general analysis of structure and dynamics of silks relying on neutron scattering techniques. The analysis of quasi-elastic and vibrational spectra will be addressed in combination with numerical modeling techniques by applying force field calculation algorithms. In addition to this, further experiments with a larger wave-vector-range using thermal neutrons and larger energy transfers with microelectronvolt resolution using advanced setups are planned. It will be particularly interesting to extend the analysis of vibrational modes in the model polymer nylon-6 by incoherent inelastic neutron scattering[70] to the dragline silk case. Moreover, neutron scattering experiments during the in-situ stretching of spider silk fibers are in preparation. This will address the question whether the macroscopic stress is reflected by an affine microscopic strain and a possible effect on the hydrogen bonds.

Acknowledgment. We gratefully acknowledge technical and engineering support by Matthias Elender (ILL). We are furthermore indebted to Martin Müller (University of Kiel, Germany) for many stimulating discussions. The Oxford contribution was supported by the British EPSRC and the AFOSR of the US.

References and Notes

(1) Xu, M.; Lewis, R. V. *Proc. Natl. Acad. Sci. U.S.A.* **1990**, *87*, 7120−7124.
(2) Gosline, J. M.; Guerette, P. A.; Ortlepp, C. S.; Savage, K. N. *J. Exp. Biol.* **1999**, *202*, 3295−3303.
(3) Hayashi, C. Y.; Shipley, N. H.; Lewis, R. V. *Int. J. Biol. Macromol.* **1999**, *24*, 271−275.
(4) Hinman, M. B.; Lewis, R. V. *J. Biol. Chem.* **1992**, *267*, 19320−19324.
(5) Gosline, J. M.; DeMont, M. E.; Denny, M. W. *Endeavour* **1986**, *10*, 37−43.
(6) Vollrath, F.; Knight, D. P. *Nature (London)* **2001**, *410*, 541−548.
(7) Li, S. F. Y.; McGhie, A. J.; Tang, S. L. *Biophys. J.* **1994**, *66*, 1209−1212.
(8) Thiel, B.; Viney, C. *MRS Bull.* **1995**, *20*, 52−56.
(9) Thiel, B. L.; Guess, K. B.; Viney, C. *Biopolymers* **1997**, *41*, 703−719.
(10) Thiel, B. L.; Kunkel, D.; Guess, K.; Viney, C. In *Biomolecular Materials by Design, MRS Symposium*; Alper, M., Bayley, H., Kaplan, D., Navia, M., Eds.; Materials Research Society: Pittsburgh, 1994; Vol. 330, pp 21−30.
(11) Thiel, B. L.; Kunkel, D.; Viney, C. *Biopolymers* **1994**, *34*, 1089−1097.
(12) Burghammer, M., Müller, M., Riekel, C., Eds.; *X-ray Synchrotron Radiation Microdiffraction on Fibrous Biopolymers Such As Cellulose and in Particular Spider Silks*; Research Signpost: Trivandrum, India, 2003; Recent Res. Devel. Macromol. Vol. 7.
(13) O'Brien, J.; Fahnestock, S. R.; Termonia, Y.; Gardner, K. H. *Adv. Mater.* **1998**, *10*, 1185−1195.

(14) Baer, E.; Hiltner, A.; Keith, H. D. *Science* **1987**, *235*, 1015−1022.
(15) Grubb, D. T.; Jelinski, L. W. *Macromolecules* **1997**, *30*, 2860−2867.
(16) Yang, Z.; Grubb, D. T.; Jelinski, L. W. *Macromolecules* **1997**, *30*, 8254−8261.
(17) Bram, A.; Branden, C.; Craig, C.; Snigireva, I.; Riekel, C. *J. Appl. Crystallogr.* **1997**, *30*, 390−392.
(18) Riekel, C.; Bränden, C.; Craig, C.; Ferrero, C.; Heidelbach, F.; Müller, M. *Int. J. Biol. Macromol.* **1999**, *24*, 187−195.
(19) Riekel, C.; Madsen, B.; Knight, D.; Vollrath, F. *Biomacromolecules* **2000**, *1*, 622−626.
(20) Riekel, C.; Müller, M.; Vollrath, F. *Macromolecules* **1999**, *32*, 4464−4466.
(21) Riekel, C.; Rössle, M.; Sapede, D.; Vollrath, F. *Naturwissenschaften* **2004**, 30−33.
(22) Riekel, C.; Vollrath, F. *Int. J. Biol. Macromol.* **2001**, *29*, 203−210.
(23) Mahoney, D. V., Eby, R. K., Kinlock, A. J. In *Proceedings of the Ninth International Conference on Deformation, Yield and Fracture of Polymers*; Kinlock, A. J.; Ed.; Institute of Materials: London, 1994.
(24) Gould, S. A. C.; Tran, K. T.; Spagna, J. C.; Moore, A. M. F.; Shulman, J. B. *Int. J. Biol. Macromol.* **1999**, *24*, 151−157.
(25) Oroudjev, E.; Soares, J.; Arcidiacono, S.; Thompson, J. B.; Fossey, S. A.; Hansma, H. G. *Proc. Natl. Acad. Sci. U.S.A.* **2002**, *99*, 6460−6465.
(26) Dong, Z.; Lewis, R. V.; Middaugh, C. R. *Arch. Biochem. Biophys.* **1991**, *284*, 53−57.
(27) Shao, Z.; Vollrath, F.; Sirichaisit, J.; Young, R. J. *Polymer* **1999**, *40*, 2493−2500.
(28) Rousseau, M. E.; Lefèvre, T.; Beaulieu, L.; Asakura, T.; Pézolet, M. *Biomacromolecules* **2004**, *5*, 2247−2257.
(29) Sirichaisit, J.; Brookes, V. L.; Young, R. J.; Vollrath, F. *Biomacromolecules* **2003**, *4*, 387−394.
(30) Liivak, O.; Blye, A.; Shah, N.; Jelinski, L. W. *Macromolecules* **1998**, *31*, 2947−2951.
(31) Beek, J. v.; Kümmerlen, D.; Vollrath, F.; Meier, B. H. *Int. J. Biol. Macromol.*, **1999**, *24*, 173−178.
(32) Kümmerlen, J.; Beek, J. D. v.; Vollrath, F.; Meier, B. H. *Macromolecules* **1996**, *29*, 2920−2928.
(33) Simmons, A.; Ray, E.; Jelinski, L. W. *Macromolecules* **1994**, *27*, 5235−5237.
(34) Simmons, A.; Michal, C.; Jelinski, L. *Science* **1996**, *271*, 84−87.
(35) Holland, G. P.; Lewis, R. V.; Yarger, J. L. *J. Am. Chem. Soc.* **2004**, *126*, 5867−5872.
(36) Bonthrone, K. M.; Vollrath, F.; Hunter, B. K.; Sanders, J. K. M. *Proc. R. Soc. London* **1992**, *248*, 141−144.
(37) Eles, P. T.; Michal, C. *Macromolecules* **2004**, *37*, 1342−1345.
(38) Eles, P. T.; Michal, C. A. *Biomacromolecules* **2004**, *5*, 661−665.
(39) Termonia, Y. *Macromolecules* **1994**, *27*, 7378−7381.
(40) Bacon, G. E. *Neutron Diffraction*; Clarendon Press: Oxford, 1975.
(41) Murthy, N. S.; Stamm, M.; Sibilia, J. P.; Krimm, S. *Macromolecules* **1989**, *22*, 1261−1267.
(42) Papanek, P.; Fischer, J. E.; Murthy, N. S. *Macromolecules* **2002**, *35*, 4175−4182.
(43) Murthy, N. S.; Akkapeddi, M. K. *Macromolecules* **1998**, *31*, 142−152.
(44) Work, R. W.; Emerson, P. D. *J. Arachnol.* **1982**, *10*, 1−10.
(45) Madsen, B.; Vollrath, F. *Naturwissenschaften* **2000**, *87*, 148−153.
(46) The ILL Yellow Book, www.ill.fr/pages/science/IGroups/yb-.pdf.
(47) Lindner, P., Zemb, T., Eds.; *Neutrons, X.-Rays and Light: Scattering Methods Applied to Soft Condensed Matter*; North-Holland: Amsterdam, 2002.
(48) Hammersley, A. In http://www.esrf.fr/computing/scientific/FIT2D/.
(49) Craig, C. L. *Spiderwebs and Silk: Tracing Evolution From Molecules to Genes to Phenotypes*; Oxford University Press: New York, 2003.
(50) Arnott, S.; Dover, S. D.; Elliott, A. *J. Mol. Biol.* **1967**, *30*, 201−208.
(51) Marsh, R. E.; Corey, R. B.; Pauling, L. *Biochim. Biophys. Acta* **1955**, *16*, 1−34.
(52) Thiel, B. L.; Viney, C. *J. Microsc.* **1997**, *185*, 179−187.
(53) Fraser, R. D. B.; MacRae, T. P. *Conformations of Fibrous Proteins*; Academic Press: New York, 1973.
(54) Thiel, B. L.; Kunkel, D. D.; Viney, C. *Biopolymers* **1994**, *34*, 1089−1097.
(55) Valluzzi, R.; Probst, W.; Jaksch, H.; Zellmann, E.; Kaplan, D. L. *Soft Mater.* **2003**, *1*, 245−262.
(56) Nelson, R.; Sawaya, M. R.; Balbirnie, M.; Madsen, A. Ø.; Riekel, C.; Grothe, R.; Eisenberg, D. *Nature (London)* **2005**, 773−778.
(57) Lotz, B.; Wittmann, J. C. In *Materials Science and Technology*; Cahn, R. W., Haasen, P., Kramer, E. J., Eds.; VCH: Weinheim, 1993; Vol. 12, pp 81−151.
(58) Gosline, J.; Denny, M.; DeMont, M. *Nature (London)* **1984**, *309*, 551−552.
(59) Miller, L. D.; Eby, R. K. *Polymer* **2000**, *41*, 3487−3490.
(60) Jenkins, P. J.; Donald, A. M. *Polymer* **1996**, *37*, 5559−5568.
(61) Vainshtein, B. K. *Diffraction of X-rays by Chain Molecules*; Elsevier: Amsterdam, 1966.
(62) Jacrot, B. *Rep. Prog. Phys.* **1976**, *39*, 911−953.
(63) Müller, M.; Czihak, C.; Vogl, G.; Fratzl, P.; Schober, H.; Riekel, C. *Macromolecules* **1998**, *31*, 3953−3957.
(64) Frische, S.; Maunsbach, A.; Vollrath, F. *J. Microsc.* **1998**, *189*, 64−70.
(65) Klug, H. P.; Alexander, L. E. *X-ray Diffraction Procedures for Polycrystalline and Amorphous Materials*, 2nd ed.; Wiley-Interscience: New York, 1974.
(66) Viney, C. *Supramol. Sci.* **1997**, *4*, 75−81.
(67) Czihak, C.; Müller, M.; Schober, H.; Heux, L.; Vogl, G. *Physica B* **1999**, *266*, 87−91.
(68) Czihak, C.; Müller, M.; Schober, H.; Vogl, G. *Physica B* **2000**, *276−278*, 286−287.
(69) Liu, L.; Faraone, A.; Mou, C.-Y.; Yen, C.-W.; Chen, S.-H. *J. Phys.: Condens. Matter* **2004**, *16*, S5403−S5436.
(70) Papanek, P.; Fischer, J. E.; Murthy, N. S. *Macromolecules* **1996**, *29*, 2253−2259.

MA0507995